

Plasma control of vortex flow on a delta wing at high angles of attack

Andrey A. Sidorenko · Alexey D. Budovskiy · Anatoly A. Maslov · Boris V. Postnikov · Boris Yu. Zanin · Ilya D. Zverkov · Victor V. Kozlov

Received: 22 January 2013 / Revised: 26 June 2013 / Accepted: 18 July 2013 / Published online: 8 August 2013
© Springer-Verlag Berlin Heidelberg 2013

Abstract The flow over a delta wing at high angles of attack is characterized by the presence of two large-scale primary vortices on the leeward side of the wing. These vortices contribute substantially to lift production at high angles of attack. Therefore, vortex breakdown, which can be induced by unfavorable pressure gradients or free-stream disturbances, can lead to an abrupt decrease in lift and to the emergence of a roll moment. Thus, the possibility of vortex flow control can be very useful. The problem of vortex flow control is investigated experimentally under subsonic flow parameters in the range of wing chord-based Reynolds number $(0.14, 0.25) \times 10^6$. A dielectric barrier discharge (DBD) is used as an active control actuator. The data obtained by means of oil flow and smoke flow visualization, surface pressure measurements, and using a particle image velocimetry technique show that the DBD can provoke early vortex bursting. Under certain conditions (discharge excitation mode and frequency), flow excitation by the discharge actuator is found to result in vortex stabilization.

Nomenclature

A_1 Primary vortex attachment line
 A_2 Secondary vortex attachment line
 C_p Pressure coefficient, $(p - p_0)/q_\infty + 1$
 c Wing root chord length (mm)

f Discharge frequency in continuous mode (kHz)
 F Pulse packet repetition frequency in burst mode (Hz)
 F^+ Reduced frequency, Fc/U_∞
 p Static pressure on the model surface (Pa)
 p_0 Total pressure (Pa)
 S_2 Secondary vortex separation line
 t Time (s)
 q_∞ Mean free-stream dynamic pressure (Pa)
 U_∞ Mean free-stream velocity (m/s)
 W Discharge power (Watt)
 x Vortex breakdown position along the wing chord (mm)
 y Vertical direction perpendicularly xz -plane (mm)
 z Transversal direction along the wing span (mm)

Greek

α Angle of attack ($^\circ$)
 ω Flow vorticity in xy -plane (1/s)
 χ Leading edge sweep angle ($^\circ$)

Subscripts

∞ Free-stream condition
0 At zero local mean velocity

1 Introduction

The main feature of the flow on the leeward side of a delta wing at high angles of attack is the formation of two primary large-scale vortices (Fig. 1). Each vortex is able to generate a low-pressure region on the upper surface of the wing and create additional lift. The contribution of the vortex-induced lift to the total lift increases with increasing angle of attack and sweep angle of the delta wing and can reach up to half of the total lift or be more than twice as high as that of a two-dimensional airfoil at high angles of

A. A. Sidorenko (✉) · A. D. Budovskiy · A. A. Maslov · B. V. Postnikov · B. Yu. Zanin · I. D. Zverkov · V. V. Kozlov
Khristianovich Institute of Theoretical and Applied Mechanics,
Siberian Branch of Russian Academy of Sciences
(ITAM SB RAS), Institutskaya str. 4/1,
Novosibirsk 630090, Russia
e-mail: sindr@itam.nsc.ru

A. D. Budovskiy
e-mail: budovsky@itam.nsc.ru

attack (Wentz and Kohlman 1968; Lee and Ho 1990). Another crucial feature of the flow is a vortex breakdown phenomenon that appears at large angles of incidence. The phenomenon is of great practical importance especially in the field of aeronautics, as it is a limiting factor on the operating attitude of slender-winged flying vehicles (Hall 1972). Therefore, the ability to manipulate and ultimately control vortex flow over a delta wing is of vital importance, because these vortices mainly determine the aerodynamics of such wings at high angles of attack.

Nowadays, there are many experimental investigations concerning vortex flow control on delta wings by means of various mechanical (flaps, strakes, etc.) and pneumatic devices (blowing, suction, etc.) or their combinations (Marchman 1981; Lamar 1980; Gursul et al. 1995; Mitchell et al. 2000; Owens and Perkins 1995; Guy et al. 1999). Using plasma discharge actuators for flow control may be advantageous compared to the above techniques. These actuators have simple construction, do not change the aerodynamic shape or influence the wing functionality when they are not in use, allow for smooth variations of forcing frequency and power, and can be used for closed loop feedback control.

This type of flow-control devices was proposed by Roth and Wilkinson (1998), and it is well known to introduce not only direct flow acceleration but also periodic disturbances due to periodic flow acceleration in the boundary-layer region, as well as acoustic disturbances (Roth and Dai 2006; Baird et al. 2005). The periodic nature of the flow generated by DBD caused by the discharge is in fact self-limited. This self-limiting behavior is caused by charge buildup on the dielectric surface when the applied voltage is negative (Enloe et al. 2004). This leads to decreasing of the electric field intensity and thus to decreasing the velocity of the flow generated by the discharge. In contrast,

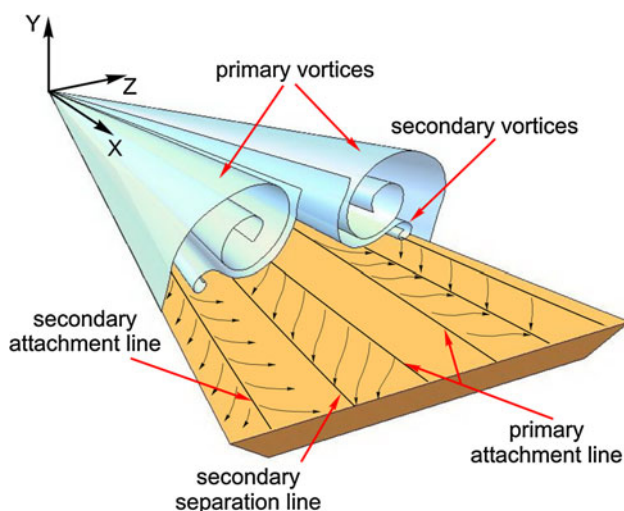


Fig. 1 Flow topology on a delta wing at a high angle of attack

when the voltage reverses, the charge transferred through the plasma is limited to that deposited on the dielectric surface. Moreover, in the paper of Forte et al. (2007), it was shown using time-resolved LDV measurements that the DBD actuator generates a pulsed velocity at the same frequency as the applied high voltage, and that the negative half-period induces more velocity than the positive one. These measurements proved that the DBD does not act in the same way during the negative and positive half-cycles, which is fully consistent with the observations of Enloe et al. (2004).

The experimental studies performed by Greenblatt et al. (2008) as well as by Kwak and Nelson (2010), for example, demonstrate the successful application of this type of plasma actuators for vortex flow control on delta wings at Reynolds numbers $\leq 0.075 \times 10^6$ and $\leq 0.1 \times 10^6$, respectively. In the paper of Greenblatt et al. (2008), the experiments were performed using a model of a delta wing with a 200-mm chord, a 60° sweep angle, and a sharp leading edge. The encapsulated and exposed electrodes were mounted on opposite surfaces of the wing and produced a plasma-induced jet inboard from the leading edge. A clear dependency of a vortex stabilization effect on the reduced frequency F^+ and the duty cycle for a pulsed plasma actuation was demonstrated in the experiments; and the most pronounced effect was observed at $F^+ \sim 1$. The opportunity have influence in a periodical manner is of great importance because the value of flow velocity generated by DBD is actually limited and rather small. This is the reason why the mechanism of influence connected with direct flow acceleration can be ineffective under higher free-stream velocities.

The vortex breakdown phenomenon is caused by two main factors, which are the adverse pressure gradient to which the vortex is submitted and its swirl intensity which cannot go beyond a critical value (Delery 1994). The unfavorable pressure gradient is not that harmful. It is always present at the trailing edge of the wing and becomes gradually enhanced with increasing angle of attack. Therefore, the influence of this factor on vortex breakdown is fairly predictable. Another factor is the sensitivity of vortex flow to free-stream disturbances (Mabey 1997). This factor is more dangerous as it can lead to a sudden decrease in lift and, moreover, to the emergence of a roll moment. Thus, the sensitivity of vortex flow to external disturbances allows the DBD to be used for vortex breakdown control. Moreover, there are instabilities inherent in the vortex flow (the feeding-sheet instability, the vortex breakdown instability, and the near-wake instability) that were demonstrated in the review paper of Rockwell (1993). Therefore, the excitation of vortex flow at appropriate frequencies can give the expected results, allowing manipulating and ultimately controlling of the flow.

The paper deals with an application of the dielectric barrier discharge to vortex flow control on delta wings in the range of Reynolds numbers higher than has previously been investigated. The control strategy in this study is mainly focused on changing the vortex breakdown position by means of excitation of the flow on the leeward surface of the wing by periodic disturbances of small intensity generated by DBD actuators.

2 Experimental setup

2.1 Wind tunnel

The experiments were conducted at ITAM in a T-324 low-turbulence subsonic wind tunnel which velocities ranging from 3 to 33 m/s. The wind tunnel has a $1\text{ m} \times 1\text{ m} \times 4\text{ m}$ square test section. The turbulence intensity is sufficiently low ($Tu = 0.04\%$), which facilitates extrapolation of wind-tunnel data to flight conditions and allows the influence of DBD-induced disturbances on vortex breakdown phenomenon to be studied.

2.2 Experimental model

Available publications concerning vortex breakdown on delta wings with a sharp leading edge under subsonic flow conditions show that vortex bursting occurs at a certain critical angle of attack, which depends on the aspect ratio of the wing and almost does not depend on the Reynolds number (Johnson et al. 1976; Roos and Kegelman 1990; Traub and Galls 1996). With allowance for the test-section geometry and the blockage ratio, an experimental model was prepared for wind-tunnel experiments. It is a delta wing with a leading edge sweep angle of $\chi = 65^\circ$, chord length $c = 300\text{ mm}$, aspect ratio 1.865, and thickness 30 mm (Fig. 2). The leading edges of the delta wing are bevelled to 30° . The model was made of a dielectric material (Plexiglas). The delta wing was installed in the wind-tunnel test section on the pylon of the mechanism for varying the angle of attack (α -variation mechanism), so the angle of attack α could be varied in the range from 0° to 45° .

2.3 DBD actuators and high voltage equipment

The design of DBD actuators is similar to that used in most studies dealing with DBD flow control (Moreau 2007) (Fig. 3). The DBD electrodes were made of a $50\text{-}\mu\text{m}$ -thick adhesive aluminum film. The encapsulated electrode is approximately 7 mm wide; the exposed electrode (also 7 mm wide) is glued with a 1-mm overlap. The barrier was made of three layers of a PVC adhesive film with an overall

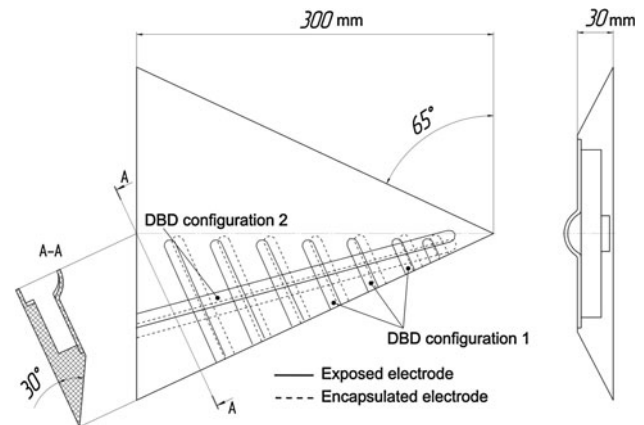


Fig. 2 Delta wing model with plasma actuator configurations used in the experiments

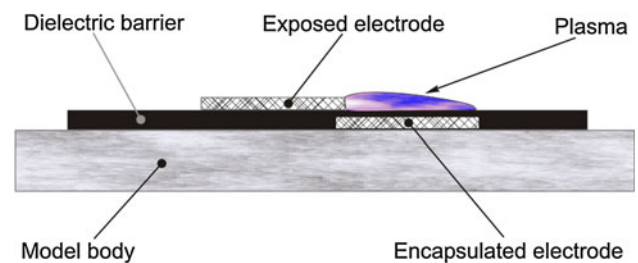


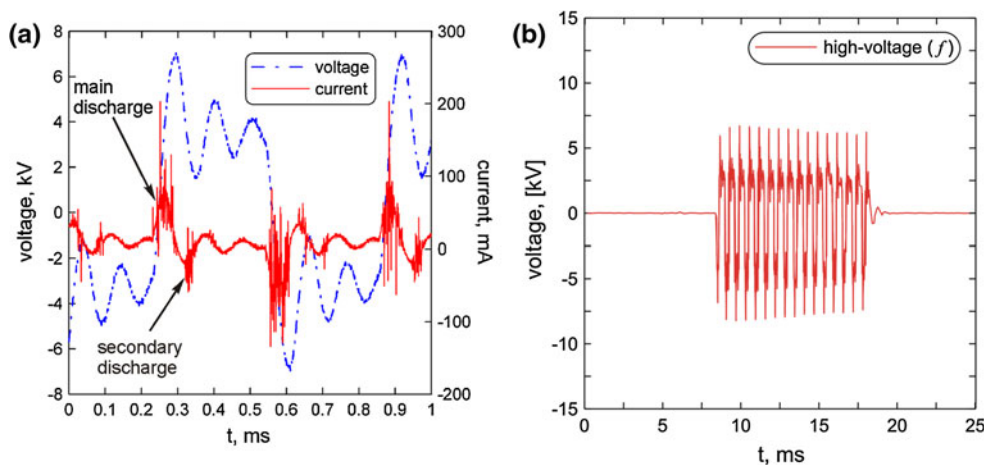
Fig. 3 DBD plasma actuator

thickness of $240\text{ }\mu\text{m}$. DBD actuators can be placed at various places on the model surface. In the present study, various DBD configurations were tested but only two of them were found to result in the expected flow control. These configurations are shown in Fig. 2. It has to be noted that the number of operated electrodes in the case of configuration 1 was varied during the experiments from 1 to 7. However, all the notable data concerning DBD configuration 1 presented here were obtained for the case of 7 excited electrodes.

The DBD power supply (High Voltage Generator) used in the experiments was the same as that used in our earlier investigations (Maslov et al. 2008). The HVG was optimized for effective operation (internal loss of 5–7 %) in the frequency range 0.5–5 kHz.

Voltage and current pulses were measured by means of two-channel 60 MHz TDS 2002 and four-channel 200 MHz TDS 2024B Tektronix oscilloscopes, 75 MHz Tektronix P6015A high voltage probe, and 60 MHz Tektronix P6021 current probe. An example of measured high voltage and current in 1.6-kHz pulses (continuous mode) is shown in Fig. 4a. Such a form of the voltage is caused by HVG electric circuit. The circuit consists of an inverter that supplies the high voltage transformer by square wave signal. This circuit was chosen due to its simple construction that gives certain benefits in terms of the weight of the high

Fig. 4 Voltage and current pulses on DBD actuator excited in continuous mode ($f = 1.6$ kHz, $W = 60$ W/m) (a) and for the discharge excited in burst mode ($f = 1.6$ kHz, $F = 40$ Hz, $W = 24$ W/m) (b)



voltage equipment. The latter is of great importance as the HVG was initially oriented for performing flight experiments where the problem of weight is a crucial question (Sidorenko et al. 2008, 2012). The HVG + DBD system is in fact an oscillating loop and therefore its natural frequency depends on the actuator's geometry (length, barrier thickness and material, length of leads, etc.). In the present experiments, the natural frequency of the high-voltage part of the circuit was not matched with the frequency f of the driving generator. Some secondary oscillations were observed during each half-period corresponding to self-induced oscillations of the HVG + DBD system. It can be seen that the main plasma discharge appears at the beginning of each half-period (seen as a series of current spikes). A secondary discharge of negligible intensity formed at the beginning of secondary pulses.

The HVG can also operate in burst mode. In the experiments, the high voltage with 7 kV amplitude and frequency $f = 1.6$ kHz was gated by the lower frequency F to initiate burst mode. The average power of the discharge does not depend on the frequency F if the duty cycle is constant. In the present experiments, the duty cycle was equal to 0.4 and, in the burst frequency range from 5 to 100 Hz, the electric power of the discharge was constant and equal to 24 W/m with 5 % accuracy.

In addition, to obtain information on the value of the flow velocity generated by DBD under excitation conditions corresponding to those presented in Fig. 4a, measurements by means of a Pitot tube were carried out. In the test case, the DBD actuator was installed on a flat plate made from plexiglass and the length of the actuator corresponded to the total length of actuator configuration 1 and was approximately 0.4 m. The measurements were performed at approximately 7 mm downstream of the leading edge of DBD's exposed electrode close to the surface. The data obtained showed that the value of average flow velocity generated by DBD is about 3 m/s. The

actuator induces average flow directed from the exposed electrode towards to the encapsulated one.

3 Measurement techniques

3.1 Pressure measurement system

Instead of the traditional surface pressure measurement technique with pressure taps and numerous sensors, an alternative method was used to reach a better space resolution on the entire surface of the model. The pressure distribution on the leeward side of the model was measured by a surface pressure probe made of stainless steel tube of 0.8 mm in diameter. The pressure tap hole of the probe was perpendicular and directed to the wing surface. The probe was pressed to the wing surface and thus measured local static pressure in the boundary layer region (Fig. 5).

The probe was connected to an Omega PX2650-10D5 V (differential pressure gauge with a range of 0- to 10-inch H₂O with a 0.2- to 5.2-V output), and the pressure was measured as the difference between the total pressures p_0 measured by a Pitot tube placed in the flow upstream of the wing and by the above-described probe p . The probe was moved along the surface by means of a three-component traversing gear. The accuracy of the pressure measurements by such a probe was estimated in separate tests in comparison with the traditional pressure tap technique and was found to be about 5 % for the present flow conditions (Zverkov et al. 2008).

3.2 Flow visualization

To obtain information on the mean flow and observe vortex evolution with increasing angle of attack, oil flow and smoke flow visualization was used in the experiments. In the tests, we used a mixture of fluorescent dye and kerosene

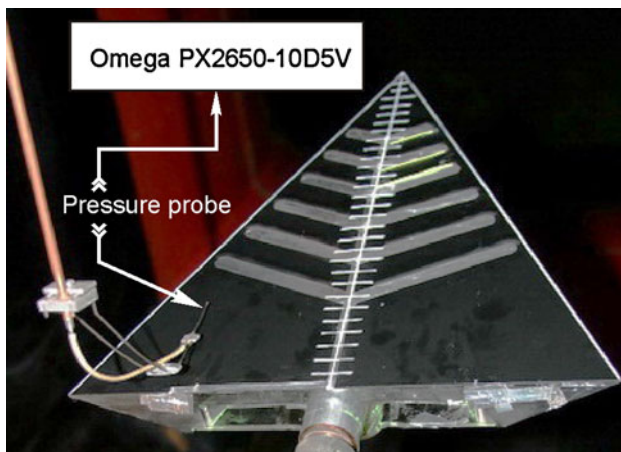


Fig. 5 The model with a probe for near-surface pressure measurements

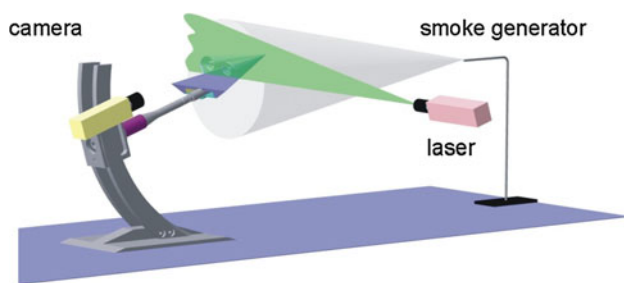


Fig. 6 Smoke flow visualization scheme

brushed on the model surface; the strokes were oriented across the main flow direction. The model was exposed in the flow until complete evaporation of kerosene and then the model was photographed. To increase the image contrast, the model surface in some cases was painted black.

Smoke flow visualization was performed by the laser sheet method, as shown in Fig. 6. A red semiconductor 25-mW continuous mode laser with a wavelength of 654 nm and optical cylindrical prism was used to create a laser sheet. The laser sheet illuminated the flow in the plane perpendicular to the model surface. The smoke was injected far upstream of the model to minimize the possible influence on the flow over the model. Video recording of the visualization was performed by means of a TV camera (25 frame/s) installed on a pylon downstream of the model. To study the vortex flow pattern in various sections along the wing chord, a scanning laser sheet method was applied. In other words, the laser sheet was gradually moved from the wing tip to the trailing edge during the experiment, thus giving an opportunity to observe the vortex flow pattern in any desired sections along the wing chord. The depth of focus of the camera lenses was enough to get sharp images without additional focus adjustment. The brightness of the

smoke visualization images gradually decreases from right to left due to laser beam expansion and its absorption by the smoke particles.

3.3 2D velocity measurements by PIV

The velocity measurements were performed by means of the PIV system POLIS¹ designed by the Institute of Thermal Physics SB RAS, Novosibirsk, Russia. The system provides the following capabilities: laser energy per pulse, 70 mJ; pulse repetition rate, 8 Hz; size of image, $1,392 \times 1,040$ pixels; and image resolution, 12 bit. The velocity field was reconstructed from tracer images by means of the cross-correlation adaptive algorithms with continuous sliding of the interrogation window, grid refinement, and deformation of the interrogation cells. The random error of the velocity vector determination in these experiments was 1–2 %.

To measure the velocity distribution, the whole test section of the wind tunnel was seeded by smoke particles of about $1 \mu\text{m}$ in size. The smoke concentration was sufficient to get contrast images of the smoke particles in the laser sheet. The experiments were done using one camera installed on the pylon downstream of the model in such a way that the plane of measurements was always normal to the model surface. The experimental setup is similar to the one used for laser sheet visualization and presented in Fig. 6. Here, a high resolution CCD camera was used instead of the analog video camera used in the smoke flow visualization tests. The PIV setup with one camera allowed the measurement of the velocity components in the plane perpendicular to the camera axis.

4 Results and discussion

DBD-assisted vortex breakdown control was studied in a range of chord-based Reynolds numbers $(0.14, 0.25) \times 10^6$. Series of preliminary tests were performed without DBD actuators. Oil flow and smoke flow visualizations by means of the laser sheet were used to obtain information on the mean flow over the delta wing and its evolution with an increasing angle of attack.

Oil flow visualization gave us an opportunity to observe such features of the flow as the attachment and separation lines. Smoke flow visualization assisted in identifying the vortex location and provided an indication of the vortex pattern. A comparison of data obtained by these two techniques contributed to a more detailed understanding of the flow structure over the delta wing.

¹ <http://www.polis-instruments.ru>.

It can be seen from Fig. 7 that a separated flow configuration with at least two vortices was formed on the leeward side of the delta wing at $\alpha = 15^\circ$. An analysis of the surface streamlines allowed us to see the primary vortex attachment line (A_1), as well as the secondary vortex separation and attachment lines (S_2 and A_2 , respectively).

Oil flow prints combined with smoke visualization for several sections are shown in Fig. 8 for two different angles of attack, corresponding to different flow regimes. The data obtained show that the position of the vortex breakdown point gradually moved upstream to the wing tip with increasing the angle of attack. For α smaller than 15° , vortex breakdown occurred somewhere downstream from the model trailing edge. When the angle of attack reached 15° , the right vortex breakdown point crossed the wing trailing edge, while the left vortex demonstrated the absence of breakdown. This tendency was observed in all the tests and could probably be attributed to inaccuracy in model positioning. It can also be noted from Fig. 8a that the secondary vortex separation lines (S_2 , see Fig. 7) are slightly curved toward the wing centerline for angles of

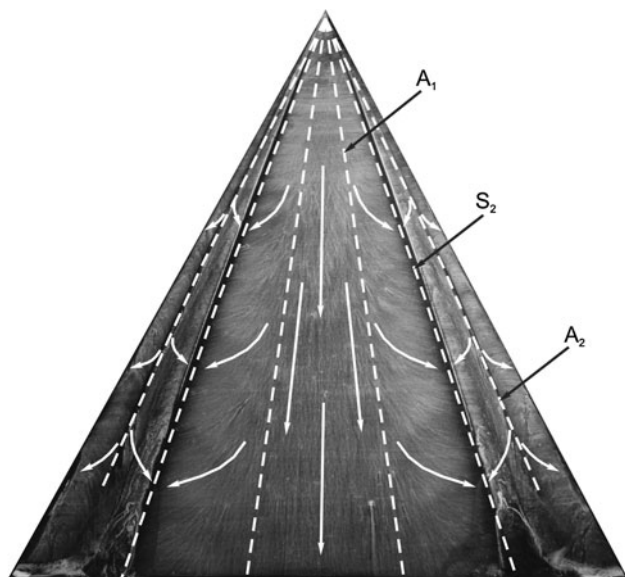
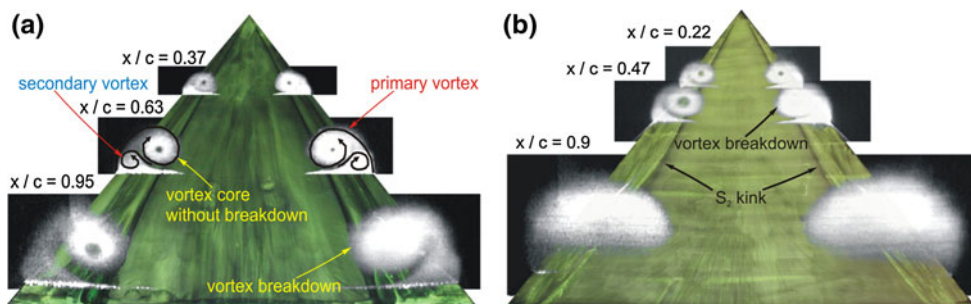


Fig. 7 Oil flow visualization print on the leeward side of the delta wing with surface streamlines ($\alpha = 15^\circ$, $U_\infty = 12$ m/s)

Fig. 8 Oil and smoke flow visualization data obtained under fixed values of free-stream velocity $U_\infty = 12$ m/s for $\alpha = 15^\circ$ (a) and for $\alpha = 22^\circ$ (b)



attack smaller than or equal to 15° . A further increase in α led to the migration of the vortex breakdown point further upstream to the wing tip. It is worth noting that the line S_2 began to bend toward the leading edge at this moment. The kink originated at $\alpha = 17^\circ$ and moved together with the vortex breakdown point further upstream toward the wing tip with increasing α (Fig. 8b).

To obtain information on the position of the secondary separation line S_2 kink along the wing chord, the following technique was applied. The photos of oil flow visualization were transformed to black-and-white mode as shown in Fig. 9. The transformation was done by means of a standard set of filters (relief, brightness, and contrast). The parameters of the filters were customized individually for each picture. It is clear from the figure that, after such a transformation, the secondary separation line can be easily recognized and its shape can be digitized using appropriate image-processing software. Thus, the digitizing procedure was performed in the coordinate system connected with the leading edge of the wing as shown in the figure. Further, the S_2 line points obtained (for clarity, not all the data points are presented in the figure) were approximated by the 6° polynomial. The S_2 kink position was determined as the extremum of the polynomial in the coordinate system connected with the leading edge. Then, the position obtained was transformed into a coordinate system connected with the wing chord.

The vortex breakdown position obtained from the smoke laser sheet visualization and the S_2 kink position obtained from oil flow visualization ($U_\infty = 12$ m/s) along the wing chord are shown in Fig. 10. It can be seen that there is a certain correlation between the vortex breakdown position and the kink of the secondary vortex separation line S_2 . Vortex bursting is known to lead to abrupt flow stagnation in the vortex core region and to vortex expansion. Thus, the secondary vortex is forced out to the leading edge, and the line S_2 is curved in the same direction. At $\alpha < 21^\circ$, the S_2 kink was located downstream from the vortex core breakdown point. This is explained by the fact that the vortex breakdown phenomenon is a non-stationary process and, therefore, the vortex breakdown position migrated within certain limits. Moreover, when the dark

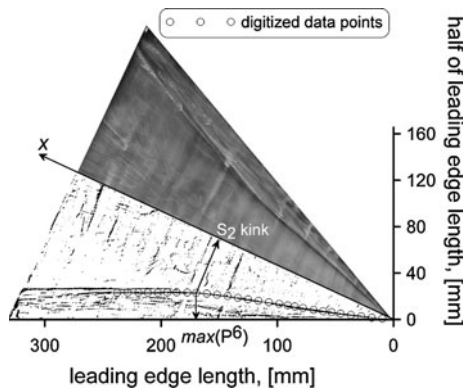


Fig. 9 Illustration of S_2 kink location definition technique

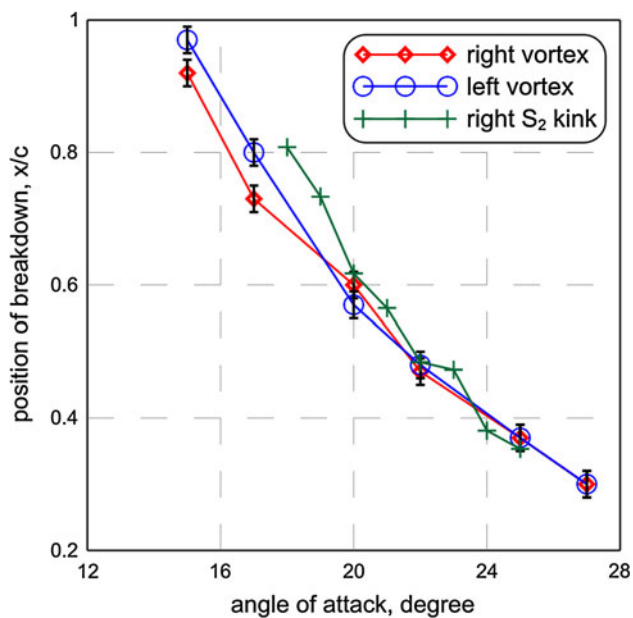


Fig. 10 Vortex breakdown and right S_2 kink locations versus angle of attack obtained under fixed value of free-stream velocity $U_\infty = 12$ m/s

vortex core disappeared, the process of flow stagnation and vortex expansion needed a certain period of time and, therefore, a certain distance before a steady burst state is reached. It can also be noted from Fig. 10 that the motion of the vortex breakdown position upstream towards the wing tip with increasing angle of attack has an approximately linear character.

In the present study, it was assumed that the main effect of the DBD on the flow is associated with the excitation of perturbations instead of acceleration of the flow in the boundary layer region. Such an excitation was therefore created on the leeward surface of the model because of the low local velocity in this region. In this case, the periodic flow induced by DBD can create perturbations of significant amplitude. It was assumed that these perturbations

convecting to the leading edge will excite the primary and secondary vortices resulting in their breakdown.

At the initial stage of the experiment, it was decided to find the most sensitive area to place plasma actuators. Linear turbulators were placed on the leeward surface of the wing to find the most effective positions for flow control from the viewpoint of the maximum shift of the vortex breakdown point. The turbulators were made of a synthetic filament with a $1\text{ mm} \times 1\text{ mm}$ square cross-section. The length of turbulators was approximately 40 mm and various configurations were tested. The most pronounced effect was observed when the turbulators were aligned perpendicularly to the wing leading edge across the vortex flow, as presented in Fig. 11f. The number of turbulators used in the experiments varied from 1 to 3. It should be noted that this kind of DBD orientation was studied using CFD modeling performed by Visbal and Gaitonde (2006) on a delta wing. The results of the flow visualization with such a configuration of turbulators are illustrated in Fig. 11. It can be seen from Fig. 11a that the vortex breakdown on the right part of the delta wing without turbulators (“clear wing”) occurred at $x/c = 0.73$. Similar results can be observed in the cases of using only one turbulator (Fig. 11d, e). The most pronounced effect was obtained in the cases of three (Fig. 11b) and two (Fig. 11c) linear turbulators installed on the right part of the wing. In these cases, the maximum shift of the vortex breakdown point toward the wing tip was observed (approximately by 15 % of wing chord). Thus, it was decided to perform the surface pressure measurements on the leeward side of the wing for two cases: clear wing (Fig. 11a) and with two turbulators used (Fig. 11c).

The data obtained are shown in Fig. 12 as the pressure coefficient $-C_p$. Figure 12a shows that the vortex flow on the clear wing is almost symmetrical, which is manifested in identical widths of the pressure peaks generated by the primary vortices. Moreover, two pressure peaks of lower intensity generated by the secondary vortices are clearly observed on both the left and right parts of the wing. The installation of turbulators as described above resulted in the right primary pressure peak becoming wider due to the breakdown of the right primary vortex (Fig. 12b). Only one secondary pressure peak can be found on the left part of the delta wing in this case (Fig. 12b). The absence of the secondary pressure peak on the right side has the same explanation as that given earlier in the case of oil flow visualization. When the primary vortex was broken down due to the influence of the turbulators, its core diameter was increased, thus forcing out the secondary vortex closer to the wing leading edge. It can be seen from the figure that the suction peak on the right side has the same order of magnitude as the left one for the case of the clear wing

Fig. 11 Smoke flow visualization data in the plane of the laser sheet obtained under fixed values of free-stream velocity $U_\infty = 12$ m/s and $\alpha = 17^\circ$ for the case of the clear delta wing (a) and with linear turbulators installed on the leeward side of the wing (b–e) (view from trailing edge)

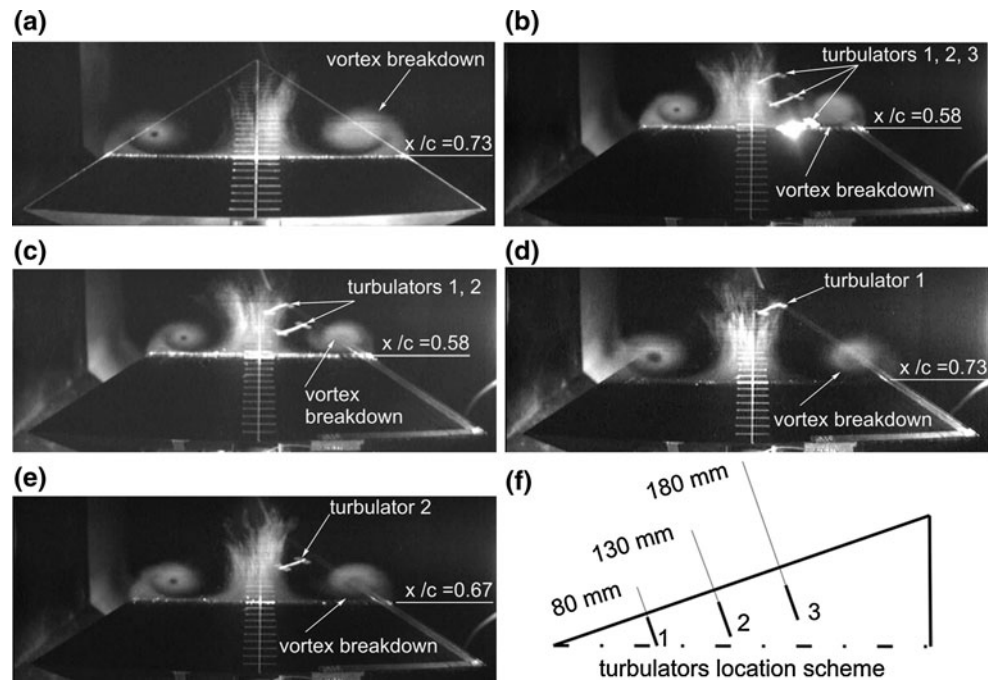
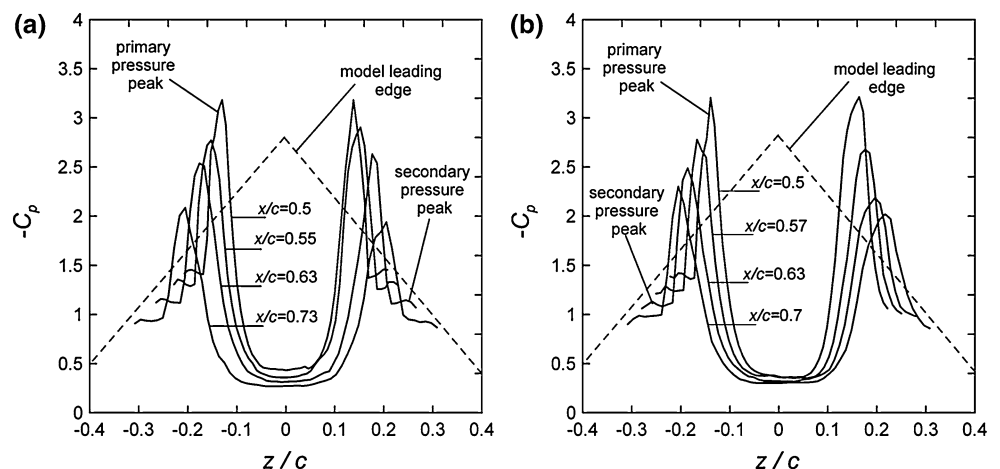


Fig. 12 Pressure coefficient distributions obtained under fixed values of free-stream velocity $U_\infty = 12$ m/s and $\alpha = 17^\circ$ for the case of the clear delta wing (a) and with linear turbulators installed on the leeward side of the wing (b)



(Fig. 12a). The $-C_p$ peaks decay in the downstream direction with the same ratio for both halves of the model in this case. And in the case of the wing with turbulators on the right side, the decay ratio on the right is higher than on the left side and than the case of the clear wing.

As the design of DBD electrodes is simple, the experiments on DBD-assisted vortex flow control were carried out with different configurations of DBD actuators. The first configuration is shown in Fig. 13. DBD actuators installed in the same manner as the turbulators were found to ensure the most effective vortex breakdown control. In this case, the DBD electrodes were perpendicular to the leading edge. The distances between the exposed electrodes were 30 mm and their total length was about 400 mm. The electrodes were arranged to generate flow acceleration or plasma propagation towards the wing tip. The DBD excitation regime

corresponds to that presented in Fig. 4a. The experiments were performed in the range of velocities $U_\infty = 7–12$ m/s at $\alpha = 0^\circ–15^\circ$. It should be noted that the velocity range was limited by the concentration of smoke particles in the flow because the smoke flow visualization was one of the main experimental techniques in the present study.

Figure 13 shows an example of the vortex flow pattern in the laser sheet plane with and without DBD excitation.

It can be seen from Fig. 13a that there are two vortices with well-defined dark cores on the left and right sides of the wing in the “DBD off” case. If the DBD was activated on the right part of the wing (Fig. 13b), only the left vortex has a core, while the right one is destroyed.

The second DBD configuration is shown in Fig. 14. In this case, the DBD actuator was placed along the secondary separation line (see Fig. 7) on the leeward side of the wing.

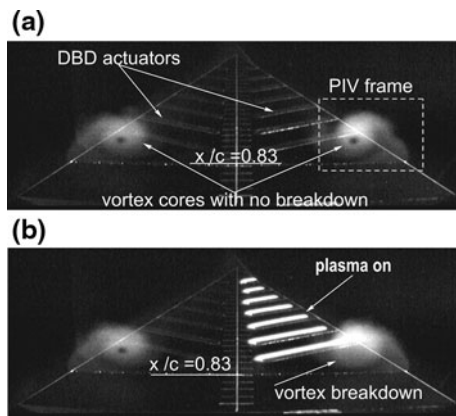


Fig. 13 Smoke flow visualization obtained for $U_\infty = 12$ m/s and $\alpha = 15^\circ$; DBD switched off (a) and DBD activated in continuous mode ($f = 1.6$ kHz, $W = 60$ W/m) (b) (view from trailing edge, DBD configuration 1)

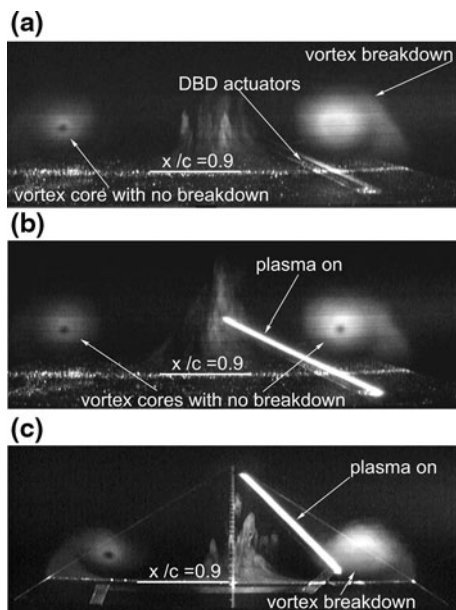


Fig. 14 Smoke flow visualization data obtained under fixed values of free-stream velocity $U_\infty = 7$ m/s and $\alpha = 15^\circ$ for the case DBD switched off (a), DBD activated in burst mode ($f = 1.6$ kHz, $F = 50$ Hz, $W = 24$ W/m) (b), and DBD excited in continuous mode ($f = 1.6$ kHz, $W = 60$ W/m) (view from trailing edge, DBD configuration 2)

It should be noted that the location of secondary separation line was determined based on the oil flow visualization data for each combination, U_∞ and α , and electrodes were suitably reinstalled before each experimental case. The electrodes were arranged to generate flow acceleration or plasma propagation towards the wing leading edge. Here, the DBD actuator was assumed to affect the shear layer between the primary and secondary vortices due to the insertion of mass flow and periodic disturbances causing

the vortex breakdown. Actually, the data obtained showed that such a configuration was ineffective from the viewpoint of vortex breakdown. Further experiments with a configuration where the DBD operation parameters (voltage, frequency, and excitation mode) were varied, however, revealed that the DBD can not only lead to vortex bursting but also to vortex stabilization. The data obtained in these experiments are shown in Fig. 14.

As can be seen from Fig. 14a, if the DBD actuator is not in use, only the left vortex has a dark core, while the right vortex is destroyed. If the DBD is activated on the right part of the delta wing, both vortices demonstrate well-defined dark cores (Fig. 14b). In other words, actuation of DBD leads to vortex stabilization on the right part of the wing. It should be noted that the effect of vortex stabilization was achieved under certain conditions: DBD was excited in the burst mode. Moreover, the effect was observed only in a narrow range of burst parameters, namely, if the pulse packet repetition frequency was equal to 50 Hz and the effect was not achieved in the range of $F = (40, 45, 47, 55, 60)$ Hz. The length of the electrode in this case was approximately 285 mm and the excitation regime corresponds to that presented in Fig. 4b. In contrast, it is seen from Fig. 14c that DBD excited in the continuous manner does not change the initial vortex flow pattern. The length of electrode in this case was approximately 245 mm and the excitation regime corresponds to that shown in Fig. 4a.

For the DBD configurations discussed above, PIV measurements were performed. Sections of measurements were defined based on the data of laser sheet visualization. Measurement regions (PIV frame) were chosen to include the leading edge of the model and the zone of the primary vortex on the right part of the delta wing (see Fig. 13a).

PIV data confirmed that excitation of the flow by the first kind of actuator (see Fig. 13) results in vortex breakdown on the right part of the model. Velocity and vorticity distributions measured in the section $x/c = 0.75$ are presented in Figs. 15 and 16.

These data were obtained by averaging 2,000 instantaneous fields. The core of the primary vortex can be easily defined on the figures. The resolution of the PIV is sufficient to resolve the secondary separation and the vortex near the leading edge. The core of the primary vortex is well pronounced in Figs. 15a and 16a and smeared in Figs. 15b and 16b due to vortex breakdown upstream for the case of activated DBD. It can be seen from the figures that downstream of the breakdown point, the vorticity in the vortex core and also the circular velocity induced suddenly decrease. This leads to the decreasing of suction on the model surface as shown above (see Fig. 12).

Data obtained for the second electrode configuration are presented in Figs. 17 and 18. The section of

Fig. 15 Velocity distribution obtained using PIV ($U_\infty = 12$ m/s, $\alpha = 15^\circ$) for the baseline flow (a) and for the flow controlled by DBD activated in continuous mode ($f = 1.6$ kHz, $W = 60$ W/m, DBD configuration 1) (b)

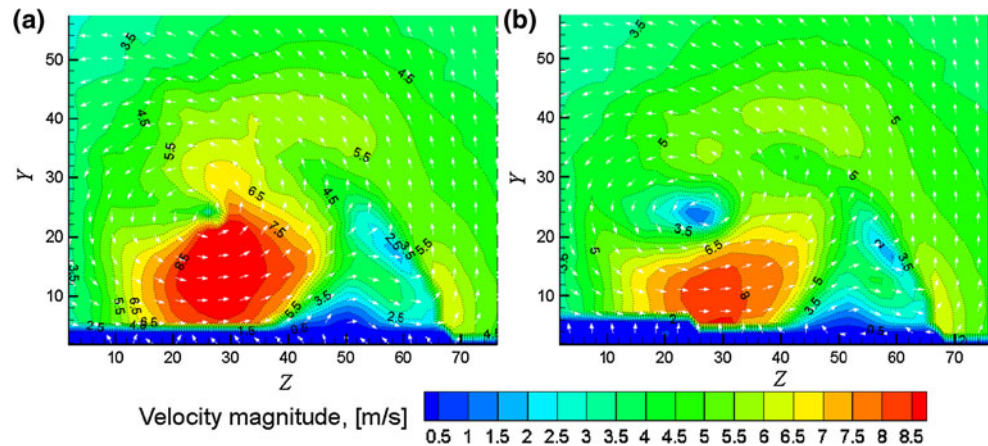


Fig. 16 Vorticity distribution obtained using PIV ($U_\infty = 12$ m/s, $\alpha = 15^\circ$) for the baseline flow (a) and for the flow controlled by DBD activated in continuous mode ($f = 1.6$ kHz, $W = 60$ W/m, DBD configuration 1) (b)

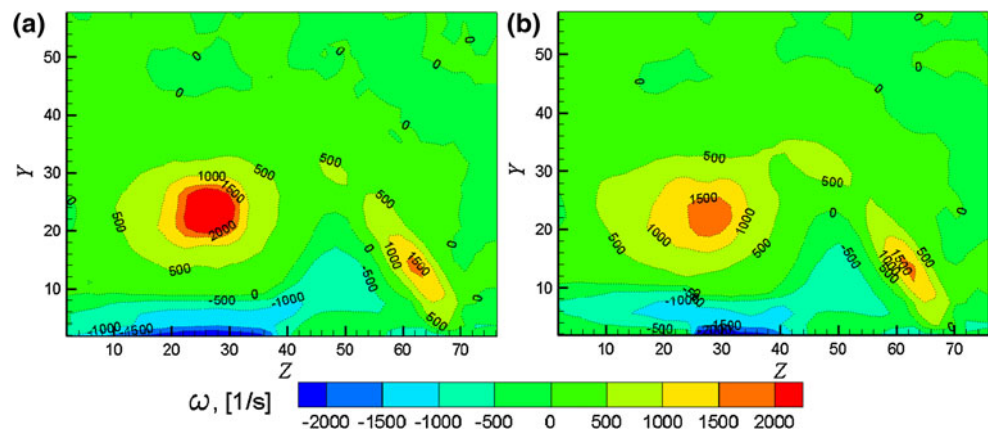
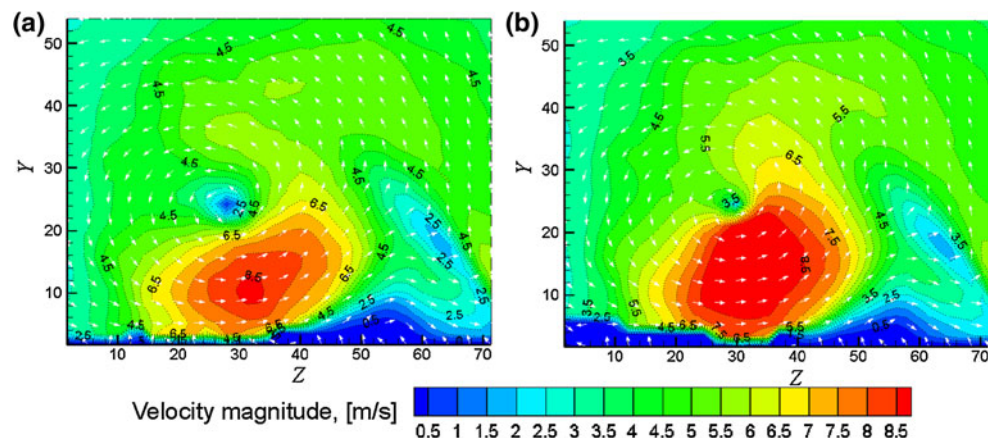


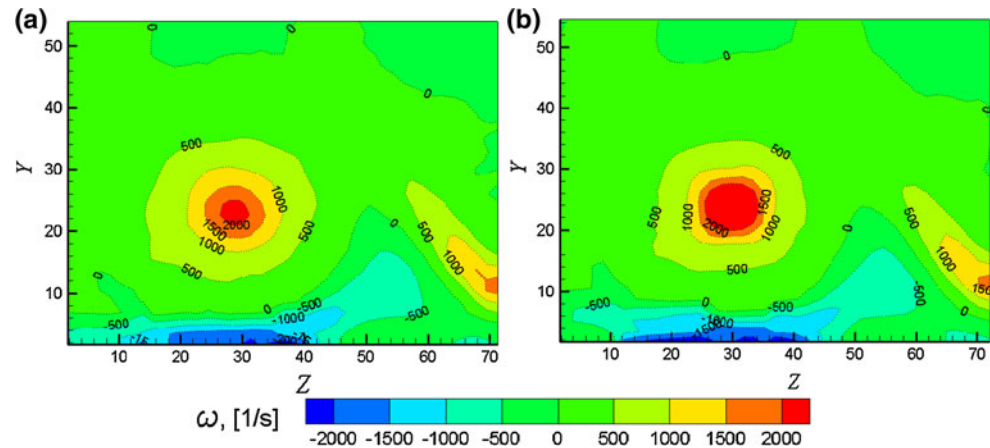
Fig. 17 Velocity distribution data obtained by means of PIV ($U_\infty = 7$ m/s, $\alpha = 15^\circ$) for the case with no excitation (a) and with DBD activated in burst mode ($f = 1.6$ kHz, $F = 50$ Hz, $W = 24$ W/m, DBD configuration 2) (b)



measurements (PIV frame) was chosen downstream of the natural breakdown point at $x/c = 0.9$. It can be seen from the figures that the vortex core recovers and the circular velocity increases for the case of excited DBD (Figs. 17b, 18b), while the initial vortex flow (if DBD was not in use) demonstrates vortex breakdown that manifested in smaller values of both velocity and vorticity magnitude (Figs. 17a, 18a).

The data on vortex stabilization obtained in the present study are consistent with the results obtained by Greenblatt et al. (2008). In the present experiments, it was also found that control was the most effective from the viewpoint of vortex stabilization at $F^+ \sim 1$ if it is calculated based on the characteristic length as $(c \cos \alpha)$ and $F^+ \sim 2$ if the root chord length is used as a characteristic scale. The presence of optimum control

Fig. 18 Vorticity distribution data obtained by means of PIV ($U_\infty = 7$ m/s, $\alpha = 15^\circ$) for the case with no excitation (a) and with DBD activated in burst mode ($f = 1.6$ kHz, $F = 50$ Hz, $W = 24$ W/m, DBD configuration 2) (b)



frequency enables us to suppose that the mechanism of vortex stabilization under discharge excitation is probably associated with suppression of some perturbations having natural frequency.

One of the characteristic frequencies of vortex flow on the delta wing can be associated with discrete vortices shedding from wing leading edge, as was shown by Gad-el-Hak and Blackwelder (1985) as well as by Payne et al. (1988). In the paper of Gad-el-Hak and Blackwelder, the empirical relationship for estimating the frequency was obtained as $f_0 = 1.3 \cdot \sqrt{U_\infty}$. For the test case corresponding to the results shown in Fig. 14, this relationship gives the value $f_0 \sim 34$ Hz while the optimum discharge frequency was $F = 50$ Hz. On the other hand, the characteristic frequency can be associated with the primary vortex precession due to the spiral type of vortex breakdown that is the predominating mechanism of vortex breakdown on delta wings (Leibovich 1984). Unfortunately, there has been no opportunity to check this assumption as the frequency mentioned was not revealed in the present study.

The explanation that the mechanism of vortex stabilization is connected with the suppression of some natural oscillations of the vortex flow can be reasonably criticized due to the control process not being synchronized with the natural vortex motion in the experiments. Therefore, another explanation can be considered. It should be recalled that the DBD actuator in the test case was installed in the secondary separation region with low flow speeds. Thus, the flow velocity generated by the DBD in this case can significantly influence the flow parameters in the boundary layer region. Hence, the mechanism of vortex stabilization can be associated with the stabilization or fixation of the secondary separation line that in turn leads to stabilization of the secondary vortex and finally to global stabilization of the whole vortex flow. Of course, this conclusion can be considered as a matter for discussion and further investigations.

5 Conclusions

The possibility of vortex flow control on the model of a delta wing was studied at a subsonic speed in the range of chord-based Reynolds numbers $(0.14, 0.25) \times 10^6$. Dielectric barrier discharge plasma on the model surface was used for vortex flow control. The effects of the discharge operating parameters and the location of the DBD actuators were studied in the experiments. It was found that DBD is able not only to influence the vortex breakdown position but also to lead to vortex stabilization when operating in the burst mode. Thus, it was demonstrated that the DBD can be successfully applied for vortex flow control on a delta wing at high angles of attack. The experimental results showed that variations of the DBD location as well as the mode of excitation exert a significant effect on the vortex breakdown control efficiency. The highest efficiency from the viewpoint of vortex breakdown was reached with the DBD was placed perpendicularly to the leading edge across the vortex flow. The configuration with DBD actuators aligned along the secondary separation line proved to be effective from the viewpoint of vortex stabilization.

References

- Baird C, Enloe CL, McLaughlin TE and Baughn JW (2005) Acoustic testing of the dielectric barrier discharge (DBD) plasma actuator. AIAA 2005-565, AIAA 43rd aerospace sciences meeting and exhibit, Reno, NV. doi:10.2514/6.2005-565
- Delery J (1994) Aspects of vortex breakdown. Prog Aerosp Sci 30:1–59. doi:10.1016/0376-0421(94)90002-7
- Enloe CL, McLaughlin TE, VanDyken RD, Kachner KD, Jumper EJ, Corke TC (2004) Mechanisms and responses of a single dielectric barrier plasma actuator: plasma morphology. AIAA J 42(3):589–594
- Forte M, Jolibois J, Pons J, Moreau E, Touchard G, Cazalens M (2007) Optimization of a dielectric barrier discharge actuator by stationary and non-stationary measurements of the induced flow

- velocity: application to airflow control. *Exp Fluids* 43(6):917–928
- Gad-El-Hak M, Blackwelder RF (1985) The discrete vortices from a delta wing. *AIAA J* 23(6):961–962
- Greenblatt D, Kastantin Y, Nayeri CN, Paschereit CO (2008) Delta-wing flow control using dielectric barrier discharge actuators. *AIAA J* 46(6):1554–1560
- Gursul I, Yang H, Deng Q (1995) Control of vortex breakdown with leading-edge devices. AIAA-95-0676, 33rd AIAA aerospace sciences meeting and exhibit, Reno, NV
- Guy Y, Morrow JA, McLaughlin TE (1999) Control of vortex breakdown on a delta wing by periodic blowing and suction. AIAA-99-0132, 37th AIAA aerospace sciences meeting and exhibit, Reno, NV
- Hall MG (1972) Vortex breakdown. *Annu Rev Fluid Mech* 4:195–218
- Johnson FT, Lu P, Brune GW, Weber JA, Rubbert PE (1976) An improved method for the prediction of completely three-dimensional aerodynamic load distributions of configurations with leading edge vortex separation. AIAA paper, pp 76–417
- Kwak D-Y, Nelson RC (2010) Vortical flow control over delta wings with different sweep back angles using DBD plasma actuators. AIAA 2010-4837, AIAA 5th flow control conference, Chicago, IL
- Lamar JE (1980) Analysis and design of stake-wing configuration. *J Aircr* 17(1):20–27
- Lee M, Ho C-M (1990) Lift force of delta wings. *Appl Mech Rev* 43(9):209–221. doi:[10.1115/1.3119169](https://doi.org/10.1115/1.3119169)
- Leibovich S (1984) Vortex stability and breakdown: survey and extension. *AIAA J* 22(9):1192–1206
- Mabey DG (1997) Similitude relations for buffet and wing rock on delta wings. *Progr Aero Sci* 33:481–511. doi:[10.1016/S0376-0421\(97\)00003-1](https://doi.org/10.1016/S0376-0421(97)00003-1)
- Marchman JF III (1981) Effectiveness of leading-edge vortex flaps on 60 and 75 degree delta wings. *J Aircr* 18(4):280–286
- Maslov AA, Sidorenko AA, et al (2008) Plasma control of flow separation on swept wing at high angles of attack. AIAA 2008-540, AIAA 46th aerospace sciences meeting and exhibit, Reno, NV. doi:[10.2514/6.2008-540](https://doi.org/10.2514/6.2008-540)
- Mitchell AM, Molton P, Barberis D, Gobert JL (2000) Control of vortex breakdown by along the core blowing. AIAA-00-2608, AIAA fluids 2000 conference, Denver, CO
- Moreau E (2007) Airflow control by non-thermal plasma actuators. *J Phys D Appl Phys* 40:605. doi:[10.1088/0022-3727/40/3/S01](https://doi.org/10.1088/0022-3727/40/3/S01)
- Owens DB, Perkins J (1995) Vortex suppression on highly-swept wings by suction boundary-layer control. AIAA 95-0683, 33rd aerospace sciences meeting and exhibit, Reno, NV
- Payne FM, Ng TT, Nelson RC, Schiff LB (1988) Visualization and wake surveys of vortical flow over a delta wing. *AIAA J* 26(2):137–143
- Rockwell D (1993) Three-dimensional flow structure on delta wings at high angle-of-attack: experimental concepts and issues. AIAA 93-0550, 31st aerospace sciences meeting and exhibit, Reno, NV
- Roos FW and Kegelman JT (1990) An experimental investigation of sweep angle influence on delta-wing flows. Technical report AIAA 90-0383
- Roth JR, Xin Dai (2006) Optimization of the aerodynamic plasma actuator as an electrohydrodynamic (EHD) electrical device. AIAA 2006-1203, AIAA 44th aerospace sciences meeting and exhibit, Reno, NV. doi:[10.2514/6.2006-1203](https://doi.org/10.2514/6.2006-1203)
- Roth JR, Wilkinson SP (1998) Boundary layer flow control with a one atmosphere uniform glow discharge surface plasma. AIAA-98-0328, AIAA 36th aerospace sciences meeting and exhibit, Reno, NV. doi:[10.2514/6.1998-328](https://doi.org/10.2514/6.1998-328)
- Sidorenko AA, Budovsky AD, Pushkarev AV, Maslov AA (2008) Flight testing of DBD plasma separation control system. AIAA 2008-373, AIAA 46th aerospace sciences meeting and exhibit, Reno, NV. doi:[10.2514/6.2008-373](https://doi.org/10.2514/6.2008-373)
- Sidorenko AA, Budovsky AD, Polivanov PA, Maslov AA (2012) Study of dielectric barrier discharge in flight experiments. 16th international conference on the methods of aerophysical research (ICMAR'2012) (Kazan, Russia, 19–25 Aug, 2012): abstracts. Pt.II. -Kazan, 2012, pp 251–252
- Traub LW, Galls LW (1996) Reynolds number effects on vortex breakdown of a blunt-edged delta. *J Aircr* 33(4):835–837
- Visbal MR, Gaitonde DV (2006) Control of vortical flows using simulated plasma actuators. AIAA 2006-505, AIAA 44th aerospace sciences meeting and exhibit, Reno, NV. doi:[10.2514/6.2006-505](https://doi.org/10.2514/6.2006-505)
- Wentz WH, Kohlman DL (1968) Wind tunnel investigations of vortex breakdown on slender sharp-edged wings. Technical report FRL 68-013, University of Kansas Center for Research, Inc.
- Zverkov ID, Zanin BV, Kozlov VV (2008) Investigation of disturbances growth in boundary layers on classical and wavy surface wings. *AIAA J* 46:3149–3158. doi:[10.2514/1.37562](https://doi.org/10.2514/1.37562)